Estimation of the Sea-State Bias in Radar Altimeter Geosat Data from Examination of Frontal Systems

J. F. MINSTER, D. JOURDAN, Ch. BOISSIER, AND P. MIDOL-MONNET

Group de Recherche de Geodesie Spahale, Unite Mixte de Recherche CNES, Avenue Edouard Belin, Toulouse, France

13 November 1990 and 9 July 1991

ABSTRACT

The sea-state bias is the deviation of the sea surface height as seen by a satellite altimeter due to differential scattering by the crest and troughs of waves and to oversimplifications of the radar waveform algorithms that calculate this height. Here the sea-state bias is estimated by automatically analyzing with a least-squares technique the along-track deviation of sea surface in the case of fronts of significant wave height (SWH). Twenty-two thousand profiles of 1500-km length of Geosat altimeter data are analyzed. Since a very strict selection was applied, only nine clear front situations are found. Among these, five correspond to atmospheric frontal situations as suggested by the altimetric wind profiles. The sea-state bias is of 3.6% ± 0.6% of SWH (2σ error). The four other fronts are interpreted as swell fronts: they present smaller biases of the order of 1.0% ± 1.6% of SWH. These results are in agreement with experimental studies and justify the calculation of sea-state bias as a function of sea maturity.

1. Introduction

The sea surface height (SSH) above the ellipsoid as measured by satellite altimetry is biased low because of differential scattering by crest and troughs of waves: this is called the *electromagnetic bias* (EM bias) (Yaplee et al. 1971). In addition, oversimplifications of the algorithms used for the analysis of the altimeter waveforms introduce tracker and skewness biases (see Lagerloef 1987; Stewart 1988; Chelton et al. 1989). The total effect is called the sea-state bias (SSB). At frequencies of past and planned radar altimeters (about 14 GHz), the EM bias is of the order of 2.0% ± 1.0% of the significant wave height (SWH), whether estimated by empirical studies (e.g., for the Geosat satellite altimeter data described by Cheney et al. 1987; Douglas and Cheney 1988; Cheney et al. 1989; Zlotnicki et al. 1989; Nerem et al. 1990; Fu and Glazman 1991), theoretical studies (e.g., Barrick and Lippa 1985; Srokosz 1986; Rodriguez 1988), or direct observations (e.g., Yaplee et al. 1971; Walsh et al. 1989; Melville et al. 1991; Branger et al. 1991). Note that the empirical determinations actually correspond to the SSB. It was higher, up to 7% of SWH, in the case of the Seasat altimeter data (Born et al. 1982; Hayne and Hancock 1982; Douglas and Agreen 1983). This was due to the particular ground processing of the Seasat measurements.

The uncertainty of the SSB estimation is of concern for the objectives of satellite radar altimeter missions: For example, the Topex/Poseidon altimeters will have the capacity of measuring SSH at a 2-cm precision (this is the point-measurement precision), which is required for observing the seasonal and interannual variability of the ocean dynamic topography. For large SWH values, the present uncertainty of the SSB correction is much larger than this value.

In particular, it has been increasingly emphasized that SSB cannot depend on SWH only, but also on wind speed or rather on sea maturity. This has been found by theoretical studies, tower and wind tunnel measurements, and analysis of the Geosat data (Walsh et al. 1989; Glazman and Pilors 1990; Melville et al. 1991; Branger and Ramamonjiarissoa 1991; Ray and Koblinsky 1991; Fu and Glazman 1991). For example, Fu and Glazman (1991) showed that when using an empirical *pseudo-wave age* defined as (Glazman et al. 1988)

$$\xi = 0.056\left[3.4 \times 10^5 \frac{g^2\,(\mathrm{SWH})^2}{U_{10}{}^4}\right]^{0.3}, \qquad (1)$$

the sea-state bias modeled as

$$\mathrm{SSB} = (0.013 \pm 0.005)(\xi/\xi_m)^{-0.88\pm0.37}\mathrm{SWH} \qquad (2)$$

is improved by 1.6 cm root-mean-square, as compared to the classical linear formula in SWH. (Here, g is the acceleration of gravity, U_{10} is the wind speed at 10 m expressed in meters per second, SWH and SSB are in

Corresponding author address: J. F. Minster, Observatoire Midi-Pyrenees, Groupe de Recherche de Geodesie Spatiale, Unite Mixte de Recherche CNES\CNRS 39, 18, Avenue Edouard Belin, 31055 Toulouse Cedex, France.

meters, and ξ_m is a globally averaged pseudo–wave age close to 2.3.) As an extreme, one might expect that SSB is very small for swell, as the latter is less steep and shows lower skewness than wind waves.

The empirical determination of the sea-state bias is generally obtained by regressions of the variations of SSH along collinear passes of altimeter data versus the SWH and U_{10} as measured by the altimeter. An adjustment of each height profile is first removed in order to decrease residual orbit errors. By doing so, one might alias differently the ocean signal, dominated by mesoscale variability on wavelengths less than about 700 km, and the SWH signal, which varies on all wavelengths (see Zlotnicki et al. 1989; Ray and Koblinsky 1991).

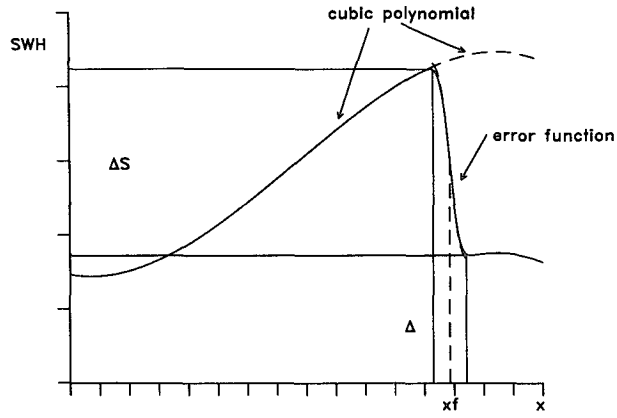

FIG. 2. Schematic representation of Eq. (3) along a significant wave height profile.

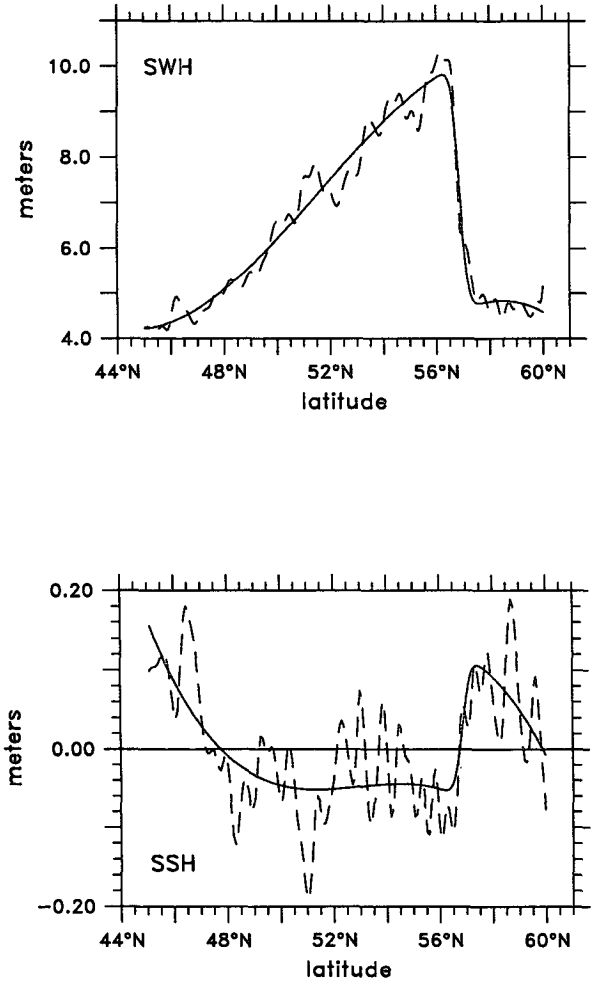

FIG. 1. Example of (a) a frontal structure of significant wave height (SWH) and (b) of the corresponding sea-state bias effect. This example has been found from Geosat data in the North Atlantic Ocean. The dashed lines correspond to filtered data, the continuous line to Eq. (3). (b) Sea surface height (SSH) residuals relative to the mean value over 2 years of repetitive measurements along the same arc.

Guymer and Srokosz (1986) suggested the use of a "short-arc technique": The sea-state bias effect is more clearly visible along a frontal structure (Fig. 1). Such SWH fronts are present in the statistical analyses such as described previously, but they probably do not dominate the result because they are rare. Guymer and Srokosz (1986) propose to use these situations because they present several advantages: they are little affected by the along-track orbit error removal, are easily separated from ocean mesoscale features, and more probably correspond to wind-wave signal because swell generally varies on long wavelengths. On the other hand, this approach can actually be sensitive to simplifications of the onboard algorithms, which do not necessarily behave correctly along a front. It is also difficult to select the frontal structures and to estimate quantitatively their amplitude and that of the corresponding sea-state bias.

In this note, we apply quantitative least-squares calculations to the short-arc technique. The Geosat altimeter data are used. A second characteristic of this work is that rather than using a statistical approach, we search for well-defined cases. In particular, by using the altimetric wind profiles and pseudo–wave age, we distinguish frontal SWH situations due to wind waves from swell fronts.

2. Methodology

In order to estimate quantitatively the amplitude of the wave front and sea-state bias, a method used by Marty and Canenave (1988) to detect fracture zones from altimeter data is used.

The along-track SWH profile is represented by a cubic polynomial and the wave front by an error function:

$$S(x) = a + b(x - x_f) + c(x - x_f)^2 + d(x - x_f)^3 + \frac{\Delta S}{2}\,\mathrm{erf}\left(\frac{x - x_f}{\Delta}\right), \quad (3)$$

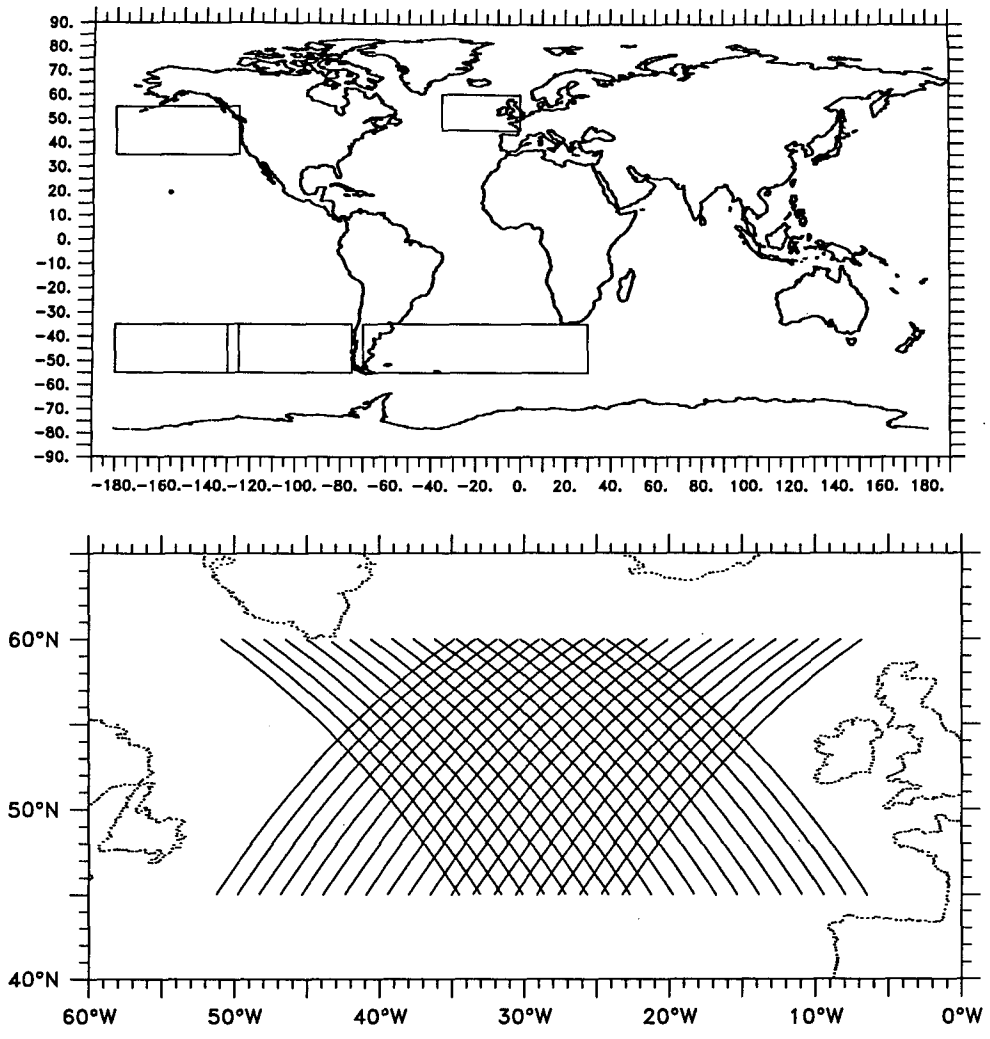

FIG. 3. (a) Areas of the Geosat data analyzed in this study. (b) Geosat arcs analyzed in the North Atlantic Ocean.

where x is the along-track position of the measurements, x_f is the position of the front, Δ is the width, and ΔS is the amplitude. Equation (3) is schematically represented in Fig. 2. There are seven unknown parameters: $S(x)$ depends linearly on five of them (a, b, c, d, and δS) and nonlinearly on x_f and Δ.

As in Marty and Cazenave (1988), these unknown parameters are estimated by a least-squares adjustment to the data. This is done iteratively by changing x_f and Δ and by fitting the linear parameters at each iteration until the best fit is achieved.

The along-track altimeter residuals are estimated by difference to a mean arc after bias and tilt removal of long wavelength orbit error, as in the classical analysis of collinear passes. The profiles of residuals are also fitted by Eq. (3); in this case, however, x_f and Δ are fixed, as determined by SWH. Then, the amplitude of the sea-state bias Δh is clearly that of a signal coincident with the SWH front. This is important because the signal-to-noise ratio of these features along SSH residual profiles is of the order of 1 only, due to the oceanic mesoscale variability (see Fig. 1).

The least-squares adjustment also provides errors on the adjusted parameters. Here they are derived from the data dispersion relative to the model profile, rather than propagated from data errors. The error is indeed dominated by the ocean mesoscale signal superimposed on the model function.

In order to select well-defined frontal situations, a series of criteria is applied.

(a) The SWH front width Δ has to be narrower than 2° in latitude along the profile.

(b) The rms of the SSH residual profile relative to Eq. (3) has to be less than 10 cm.

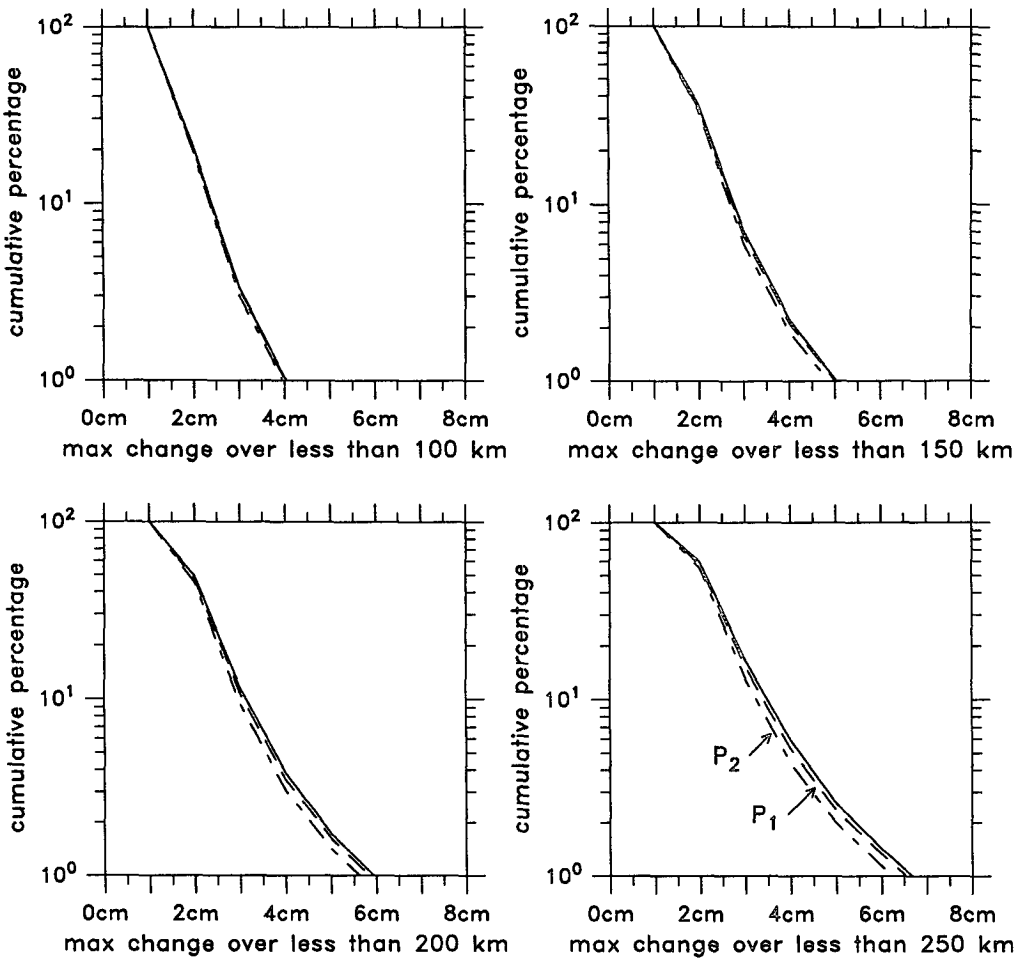

FIG. 4. Cumulative percentage of the maximum sea-state bias variations (calculated as 2% of SWH) over a given maximum distance for the 1600 arcs of Fig. 3b. These statistics are given for maximum distances of 100, 150, 200, and 250 km. Each figure gives the results for the raw profiles (continuous lines) after removal of a bias and tilt along the arc (P_1) and after removal of a second-degree polynomial (P_2).

In practice, criterion (a) ensures that the SWH profile is well described by Eq. (3) and that the sea-state bias is little affected by the bias and tilt removal of orbit error; criterion (b) ensures that the SSH sea-state bias is well separated from the mesoscale signal. The thresholds for these criteria were empirically determined in order to retain enough cases, yet obtain robust ΔS and Δh values.

Amplitude Δh is either determined from profiles of height residuals calculated relative to the mean arc (using 2 years of Geosat data) or relative to the next-in-time collinear pass. The second approach is used by Ray and Koblinsky (1991). In this case, a fraction of the mesoscale signal is removed because it is correlated from one satellite pass to the next, 17 days later. In all the cases selected here, Δh is found robust by comparison of the two approaches, meaning that the two values are within their respective 2σ error limits. Nearly all cases for which criterion (b) is set to 8 cm are robust. When the mesoscale signal is larger, the robustness criterion is particularly effective when significant mesoscale signal occurs at the position of the front.

3. Data processing

About 22 000 arcs of Geosat data from the Atlantic and Pacific oceans have been analyzed (Fig. 3). These areas have been selected because their histograms of H1/3 values (plotted for each 10° latitudinal band) showed much spreading, which suggested the occurrence of SWH fronts. The arcs are of 1500 km each and come from the first 40 cycles of the Geosat Exact Repeat Mission (Cheney et al. 1987). The geophysical corrections provided in the geophysical data records (GDRs) have been applied to altimetric height (with the exception of sea-state bias).

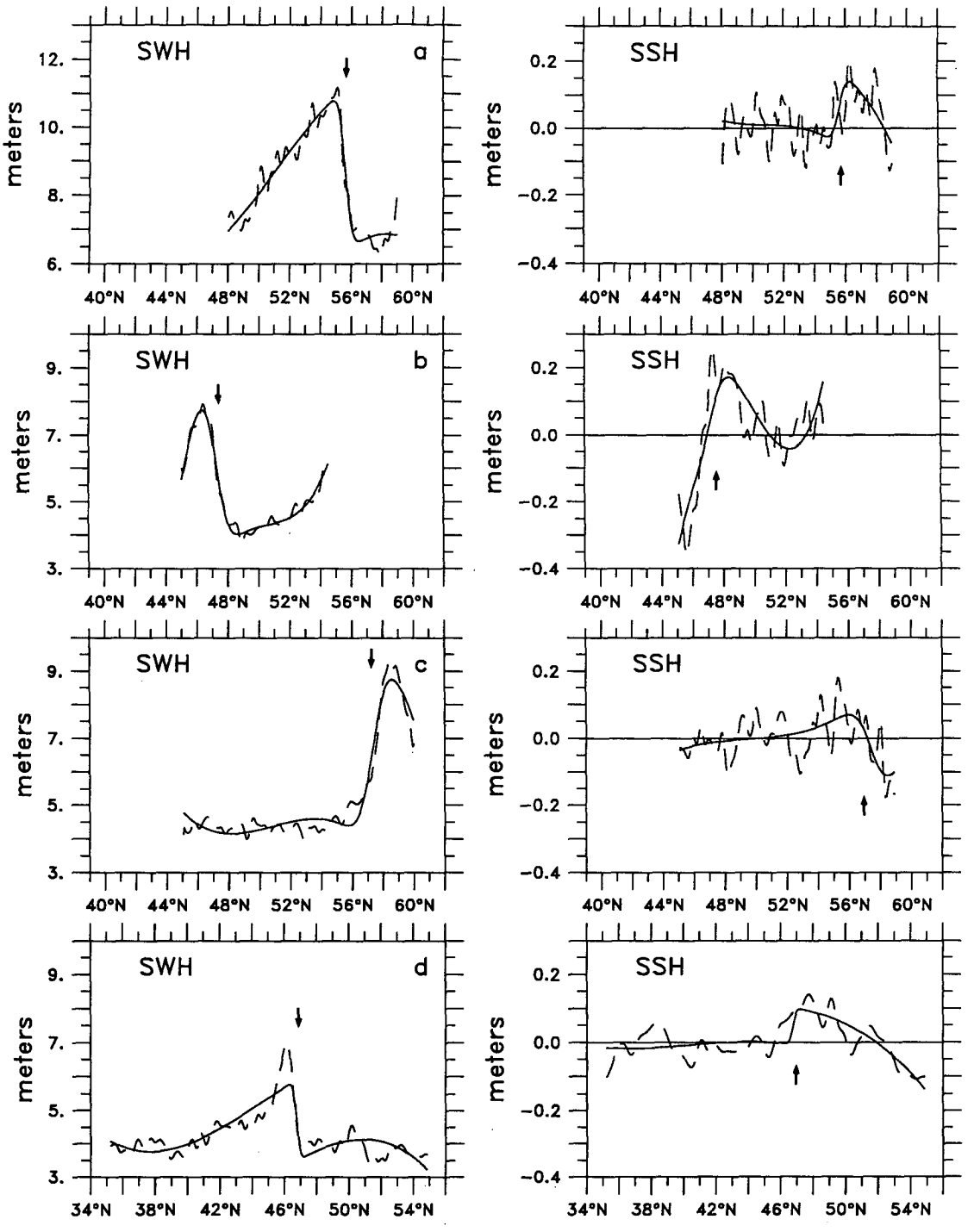

FIG. 5. Same as Fig. 1 for the eight other selected cases. SWH is the significant wave height. SSH are the sea surface height residuals. Cases (e)–(h) present small sea-state biases.

The data have been edited 1) for spikes along the height profiles larger than 80 cm, which are considered as anomalous data points, and 2) for data presenting anomalous corrections. In addition, none of the profiles show larger than 15-m SWH values.

In particular, a test had to be applied on the attitude angle as provided in the GDRs: in this dataset, the attitude angle is, most of the time, set to zero when it exceeds a value close to 1.3° (see Cheney et al. 1987). Since an attitude correction is applied to SWH and

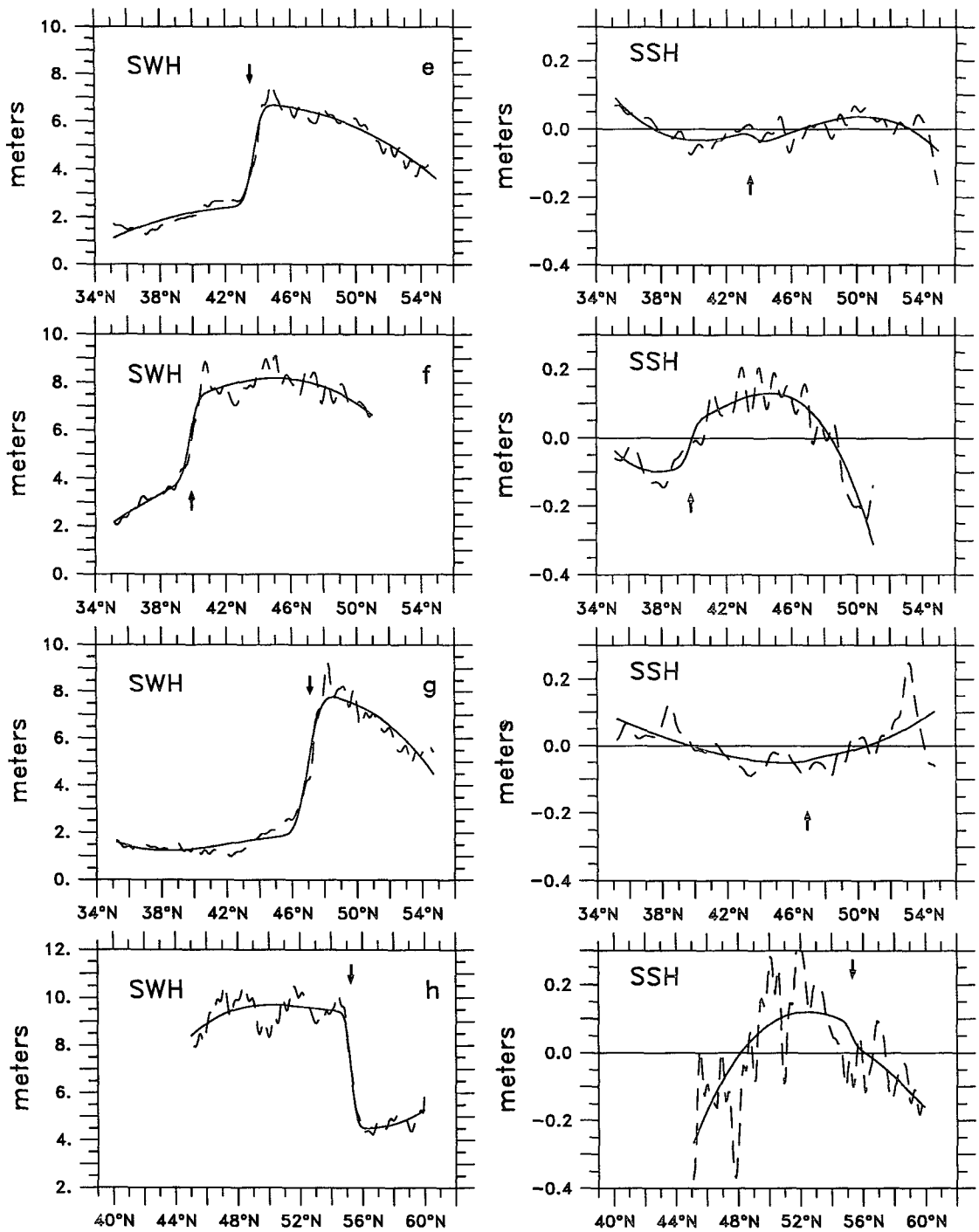

FIG. 5. (*Continued*)

SSH, this introduces artificial discontinuities along the profiles. These discontinuities are anticorrelated with an apparent coefficient larger than 10%. In addition, U_{10} is used as deduced from the altimeter data, which is (in addition to being uncertain) very sensitive to the attitude angle. It is thus a safe practice to eliminate Geosat data where the attitude angle is 0° or larger than 1.2°. This eliminates about 5% of the whole GDR dataset (C. Brossier, personal communication).

The SSH residuals are calculated relative to the mean

of up to 40 repeat passes. Only the complete arcs are used in order to avoid the introduction of jumps in this mean and thus in the residuals. In order to reduce the effect of noise, the SSH residuals are low-pass filtered by a Lanczos filter with a cutoff at 60 km. This filter did not alter the results. For more details on the technique, the reader is referred to Le Traon et al. (1990). Finally the fit to Eq. (3) and the selection according to criteria (a) and (b) were applied automatically.

4. Error analysis

One should question the sensitivity of the results to errors on the altimetric height and SWH. Indeed, these errors are significant compared to the observed features. The former is around 4 cm rms, which is the mesoscale variability as estimated in the quietest ocean areas (see Zlotnicki et al. 1989); the latter is about 50 cm (e.g., Dobson et al. 1987). Thus, the noise on the altimetric height compared to the sea-state bias is larger than the noise on SWH compared to the front amplitude. This could bias the sea-state coefficient towards low values. Ray and Koblinsky (1991) address the same question by using a Monte Carlo method and find that their coefficient might be biased low by 30%–50%. Here the effect is expected to be less severe because of the Lanczos filter and the adjustment of the whole profiles to Eq. (3).

A second difficulty in the estimation of sea-state bias is the separation from orbit errors. This is critical when it is estimated from direct regressions of altimetric height residuals versus SWH because the two parameters do not have the same wavenumber spectra. In fact, Zlotnicki et al. (1989) find that the sea-state bias coefficient decreases when the arc length used for its calculation is increased. This effect should be much less critical in this case because we are searching for signals on a well-defined short distance scale as compared to the arc length. In order to estimate the effect of the orbit error removal, statistics of the fronts are computed from the dataset of Fig. 3b. Along each pass (1600 as a whole), the maximum height difference due to sea-state bias (calculated as 2% of SWH) is calculated on all distances shorter than a given value. The population of such frontal structures is much larger than the one that follows the previous criteria. Cumulative percentages of those frontal structures are given in Fig. 4 for distances of 100 to 250 km (for example, 2.5% of the profiles show variations of the sea-state bias larger than 5 cm over less than 200-km distances). These statistics are provided for the raw data and after the removal of a first-degree (P_1) or of a second-degree polynomial (P_2). As expected, the percentage of large SSB variations is decreased after removal of P_1 or P_2. However, the amplitude of these variations is decreased by less than 10% only. This would result in an increase of the sea-state bias coefficient of the same percentage; it is clearly a minor error.

One may also suspect the effect of water vapor. It is well known that the water vapor corrections, in the Geosat GDRs, are inadequate as they are derived from the Fleet Numerical Operations Center (FNOC) meteorological model (see, e.g., Monaldo 1990; Jourdan et al. 1990). In particular, they cannot represent the atmospheric frontal structures. For example, in the North Atlantic and North Pacific oceans, SWH fronts are frequently created by cold atmospheric fronts. Behind the front, the wind, as well the SWH, are stronger; larger humidities are found in the quiet warm side of the front (see, e.g., the humidity maps of Katsaros and Lewis 1986). FNOC would smooth the corresponding water vapor structure. However, applying the exact

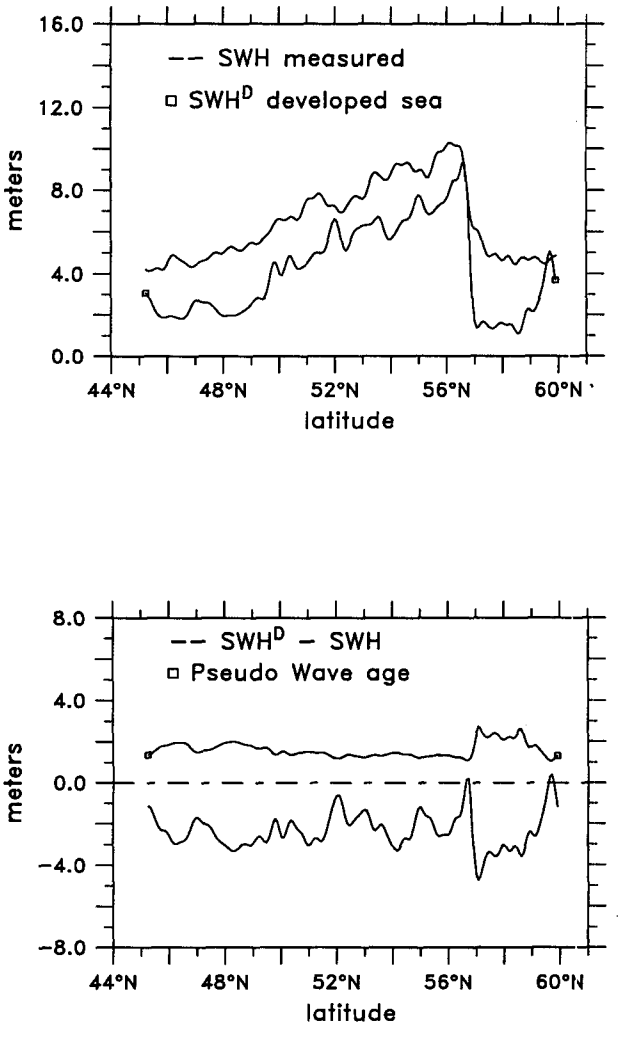

FIG. 6. Comparison between the measured SWH profile and that of developed sea (SWH^D) deduced from altimetric wind for the case of Fig. 1. (a) Profiles. (b) The difference between SWH and SWH^D and pseudo-wave age calculated by Eq. (1).

correction would increase the SSH step, attributed here to sea-state bias. The actual sea-state bias coefficient would be larger than obtained here. For a typical variation of the atmospheric water vapor of 1.0 g cm^{-2} across the front, the absence of correction would amount to an apparent decrease of the sea-state bias coefficient of 1.5% of SWH for a SWH front of the order of 4 m.

Finally, an atmospheric pressure-loading effect could be superposed, though it is not clear what the ocean response would be on the short time scales of front evolution. Assuming that this response is an instantaneous local inverse barometer effect, applying the correction would decrease the SSH step as estimated here. In the same case as before, the increase in atmospheric pressure behind the front would be of the order of 10 hPa and the absence of correction would amount to an apparent increase of the coefficient by 0.25% of SWH.

As a whole, data and processing errors can introduce some noise in ΔS and Δh of the order of 1% of SWH. Note that these errors are not included in the analysis. As the last two effects are not necessarily systematic, they might be included in the generally used statistical studies on large datasets, as described in the Introduction.

5. Analysis

As mentioned in the previous section, there are many occurrences of SWH fronts. However, only nine frontal situations satisfying the criteria given were found (Figs. 1 and 5). Some show well-defined anticorrelated ΔS and Δh values (e.g., Fig. 1. The latter was actually the first occurrence that was accidentally found and that triggered the present study). Other cases are not always so clean and show a very small Δh (e.g., Figs. 5e–h).

In order to document these cases further, the SWH profiles are compared with those for a well-developed sea and with their pseudo–wave age. For doing this, wind speed is simply derived from the automatic gain control, using the smoothed Brown algorithm (Brown et al. 1981), and SWH^D values corresponding to well-developed seas, using the relation,

$$SWH^D = 0.025 U_{10}^2, \qquad (2)$$

where SWH^D is in meters and U_{10} is the wind speed meters per second at 10 m above the surface (see Mognard 1984). Pseudo–wave age is calculated according to Eq. (1). These profiles are illustrated in Figs. 6 and 7. In most cases, the measured values are consistently larger than SWH^D, which can be attributed to deficiencies in the Brown algorithm or to swell.

Two types of profiles can be identified. The five first cases are in Fig. 6 and Figs. 7a–d. The profiles of SWH and SWH^D show similar frontal structures. The pseudo–wave age is generally high when SWH is low and gets younger ($\xi < 2$) across the front when SWH increases. Except for Fig. 7a, one generally encounters bursts of strong winds with nondeveloped seas (SWH^D larger than SWH). These cases will be called *wind-wave* fronts. For the four other cases (Figs. 7e–h), the two SWH profiles are much less or sometimes not related. The pseudo–wave age varies little across the front or gets older on the high SWH side of the front. These cases will be considered as *swell* fronts. One would expect that well-defined swell fronts be close to their exciting source. Indeed, SWH^D tends to get larger and ξ younger not very far from the fronts. Actually, in Fig. 7g, the step for $SWH - SWH^D$ is better defined than the SWH front: the actual swell fronts should have been defined by the difference $SWH - SWH^D$. Finally, it is interesting to note that three out of these four swell fronts were encountered in the Pacific Ocean.

Figure 8 represents the Δh and ΔS values with their 1σ error limits. The wind-wave fronts plot on a line of slope $-3.6\% \pm 0.6\%$. In order to take the errors into account, the regression algorithm of Minster et al. (1979) has been used. The line was forced through the origin. The error is the 2σ error propagated from the Δh and ΔS errors. The reduced χ^2 is 1.3, which suggests that the points can be indeed considered as plotting on a straight line. [For four degrees of freedom, the hypothesis that the data plot on a straight line at the 95% confidence level should be rejected if χ^2 exceeds 1.6 (see Wendt and Carl 1991).] The swell fronts tend to have a very small SSB coefficient. A regression gives a slope of $1.0\% \pm 1.6\%$, which is not different from zero. However, χ^2 is equal to 3.5 and the data points cannot be fitted to a straight line, mostly because of the case of Figs. 5f and 7f.

Thus, it is consistently found that the sea-state bias due to swell is zero or small, while the bias due to wind waves is of the order of -3.6%. Our result is in agreement with the range of values obtained in the literature. For Geosat, these empirical sea-state bias coefficients were found as 1% (Cheney et al. 1989), $1.4\% \pm 0.6\%$ (Fu and Glazman 1991), $1.9\% \pm 1\%$ to $3.5\% \pm 1.5\%$ (Douglas and Cheney 1988), $2.3\% \pm 3.4\%$ (Zlotnicki et al. 1989), $2.6\% \pm 0.2\%$ (Ray and Koblinsky 1991), and $3.6\% \pm 1.5\%$ (Nerem et al. 1990). The values would mix wind-wave and swell effects, the respective influence of which would change in various places of the ocean.

It is interesting to note that in their application of the short-arc technique to Seasat data, Guymer and Srokosz (1986) found a sea-state bias coefficient of 9%–9.8% for three situations (they do not explain how this coefficient is estimated). This is to be compared with 7% obtained with the collinear technique (Douglas and Agreen 1983). The difference between the two values is similar to that between our wind-waves value and the literature Geosat values.

By direct measurements, Walsh et al. (1989) suggest that the EM bias should be around 3.0% for 14-GHz

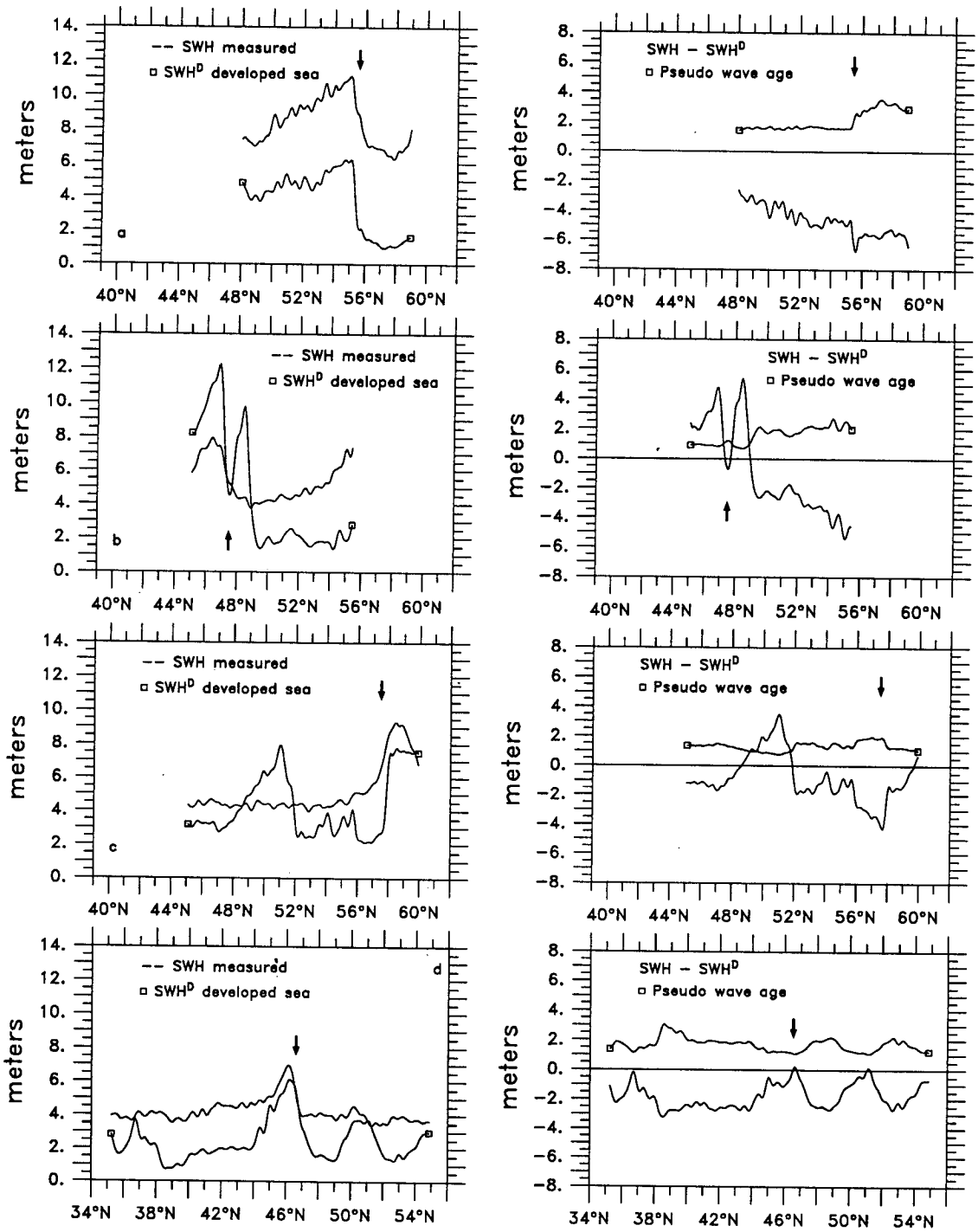

FIG. 7. Same as Fig. 6 for the cases of Fig. 5.

radars. Note, however, that they did not make direct measurements at 14 GHz; they interpolate linearly between values at 36 GHz and values at 10 GHz. The latter are very noisy: one value is at 1.4% while five others vary between 3.2% and 4.3%. In addition, at 36 GHz the Walsh et al. data suggest that the EM bias increases with wave steepness and is thus larger for nondeveloped seas. At 14 GHz, Melville et al. (1991), from tower experiments, and Branger and Ramamonjiarissoa (1991), from wind tunnel investigations, also

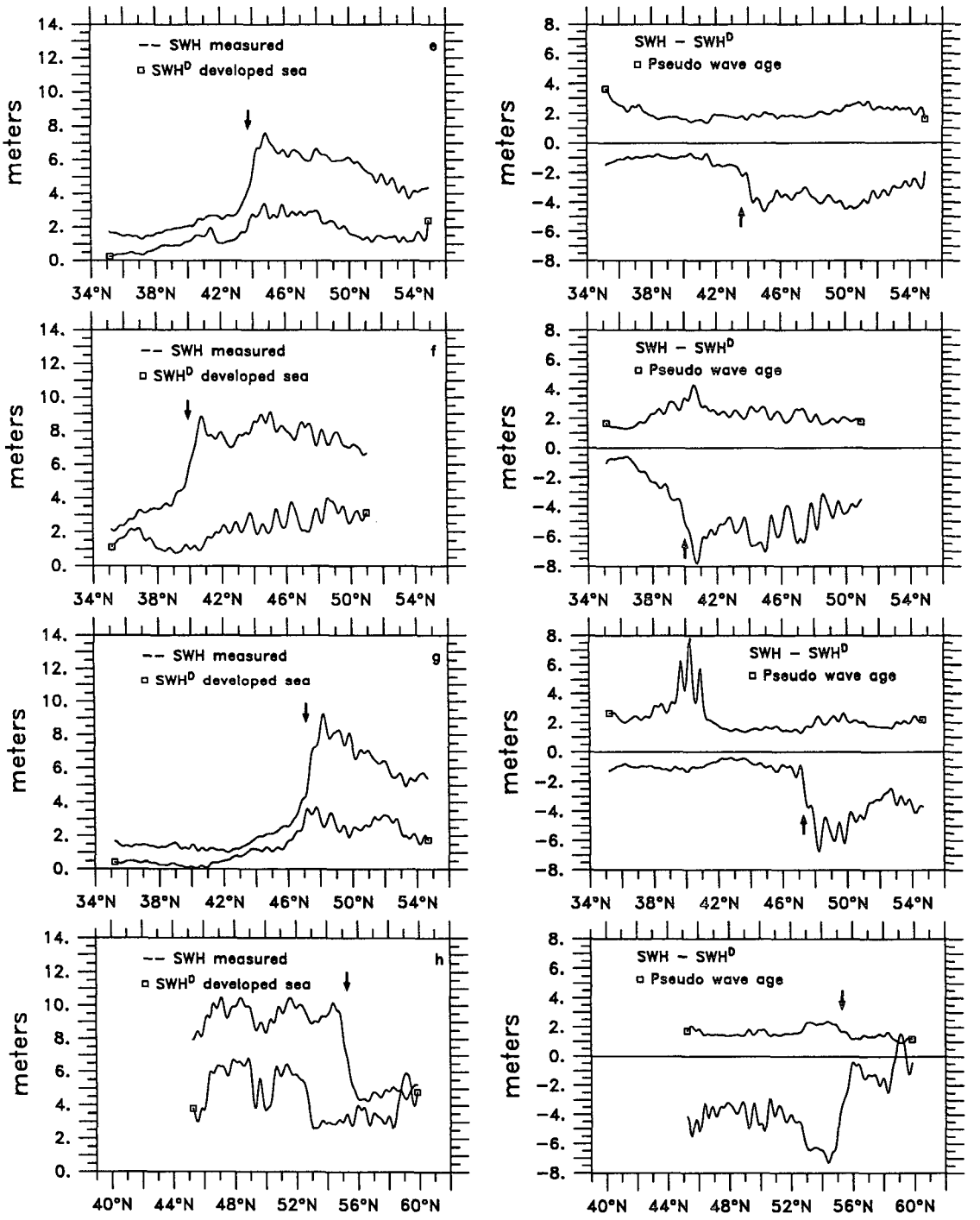

FIG. 7. (*Continued*)

find that the EM bias coefficient (i.e., the bias divided by SWH) is an increasing function of wind speed or nondimensional fetch ($s = g\,\mathrm{SWH}/U_{10}^2$). Again, our results are consistent with these measurements.

Ray and Kolbinsky (1991) proposed an "extended" sea-state bias model by calculating a regression of SSH residuals versus residuals of SWH and of SWHU_{10} (where U_{10} is the altimetric wind speed calculated using the smoothed Brown algorithm). For a given SWH, their correction increases with increasing wind speed.

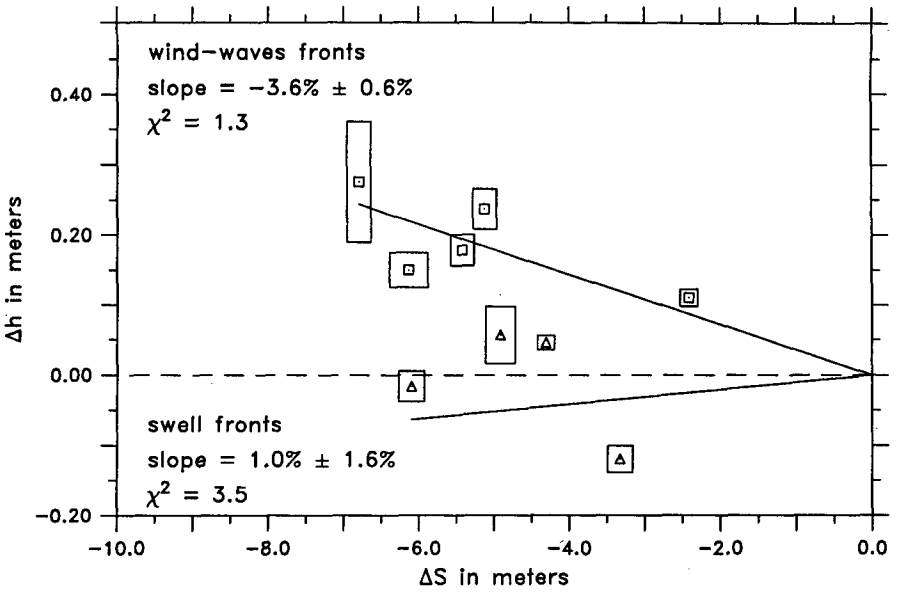

FIG. 8. Plot of the sea-state bias effect Δh versus the wave-front amplitude ΔS for the nine frontal situations satisfying the criteria (see text). Boxes correspond to errors as determined by the least-squares adjustment to Eq. (3). Squares correspond to wind-wave fronts, triangles to swell fronts. The straight lines are least-squares best fit forced to pass through the origin. The errors of the sea-state bias coefficients are the 2σ errors propagated from the error limits on Δh and Δs.

It is less than 1% for a zero wind speed and reaches about 3.5% for high wind speeds, implying nondeveloped seas. These values are consistent with ours.

In order to compare our result with that of Fu and Glazman (1991), their sea-state bias is calculated according to Eq. (2). The profiles of correction are shown on Figs. 9 and 10 where they can be compared with the SSH profiles. Except for Fig. 10f, they show similar steps. The step of the SSB correction was further calculated like that for SSH [that is, using Eq. (3) with Δ and x_f fixed by the SWH regression]. The results are shown in Fig. 11 where the error limits were derived from the ranges of values in Eq. (2) (i.e., the SSB profiles were recalculated and the step amplitudes reestimated). The agreement with the SSH values is very good and within error limits. Agreement is better than the 1% level for the SSB coefficient when the nominal values of Eq. (2) are used. By regression of the wind-wave data alone, an improved agreement is found when Eq. (2) is written as

$$\mathrm{SSB} = 0.015\,(\xi/\xi_m)^{-0.88}\mathrm{SWH}.$$

This analysis, which is not statistical in nature, demonstrates that the statistical empirical studies that include wind speed do not yield better results (i.e., lower rms of the residual sea surface heights) only because of the larger number of variables in the regression. Application of a correction such as Eq. (2) describes the range of sea-state bias situations encountered.

6. Conclusions

The variations of sea surface height as measured by satellite altimeters across fronts of significant wave height allow a quantitative estimation of the sea-state bias. By applying a very strict selection of "clean" cases (i.e., with well-defined SWH fronts and a low mesoscale dynamic topography signal), we could compare the effect of swell and wind wave. The sea-state bias due

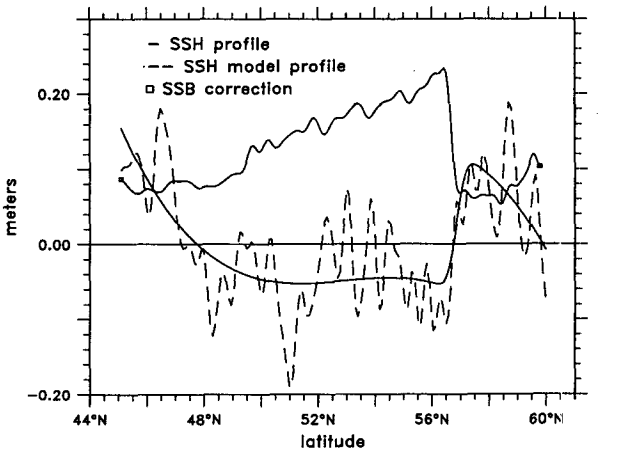

FIG. 9. Comparison of the sea surface height residuals (SSH) and the sea-state bias correction (SSB) calculated according to Eq. (2) for the case of Fig. 1.

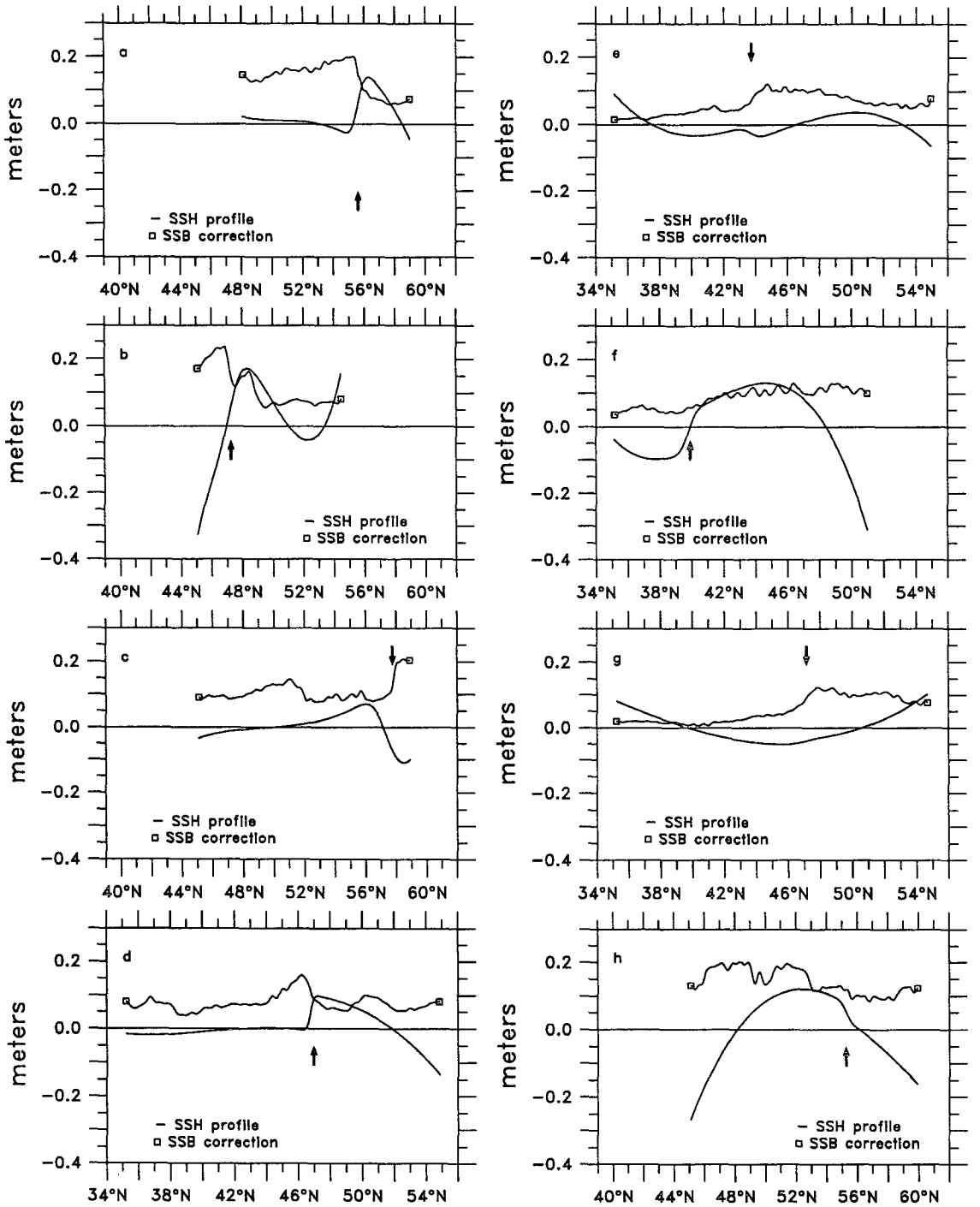

FIG. 10. Same as Fig. 9 for the cases of Fig. 5. For SSH only, the fit to Eq. (3) is shown.

to swell is small, of the order of 1.0% ± 1.6% of SWH, while that for wind waves is of the order of −3.6% ± 0.6% of SWH. This result agrees well with experimental studies that demonstrate that sea-state bias depends on SWH and wind speed. It brackets the literature empirical values estimated by regression of SWH versus SWH Geosat data. It also agrees very well with, and actually justifies, the empirical calculation of the sea-state bias as a function of sea maturity, as proposed by Fu and Glazman (1991).

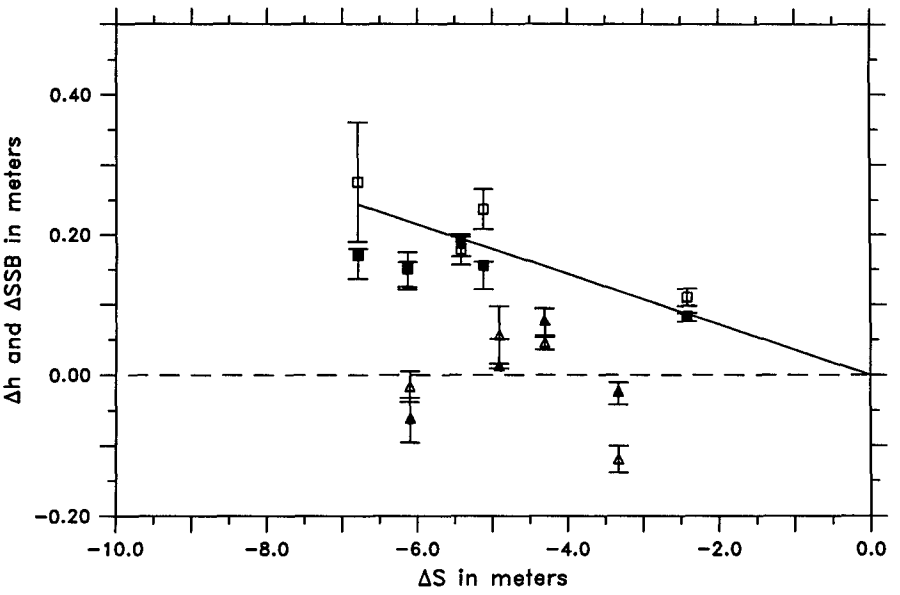

FIG. 11. Same as Fig. 8 where the step amplitudes for the sea-state bias (black symbols) is compared to those for SSH (empty symbols). Error limits for the SSB step amplitudes are derived from the range of parameters in Eq. (2). The straight line is the same as in Fig. 8.

Unfortunately, only 9 cases out of 22 000 profiles were found. The most serious difficulty of this approach is in this small number. In particular, it was not possible to analyze "intermediate" cases in terms of mixture of swell and wind waves and in terms of degree of maturity of sea state. We think that if one is to relax the selection criteria in order to increase the number of situations, it is better to use along-track statistical methods as usually done, since they provide much larger datasets. The technique used here is rather a validation of the above technique.

Acknowledgments. We thank Cl. Brossier for very helpful management of the Geosat data, M. C. Rouquet for the software for extracting sea surface height residuals, and J. C. Marty for the software for estimating the frontal parameters.

REFERENCES

Barrick, D. E., and B. J. Lipa, 1985: Analysis and interpretation of altimeter sea echo. *Adv. Geophys.*, **27**, 60–69.

Born, G. H., M. A. Richards, and G. W. Rosborough, 1982: An empirical determination of the effects of sea-state bias on Seasat altimetry. *J. Geophys. Res.*, **87**, 3221–3226.

Branger, H., and A. Ramamonjarissoa, 1991: Caractérisation du biais électromagnètique en fonction du champs de vogue. Rapport final CNES 90/800/85h, Institut de Mécanique Statistique de la Turbulence, 170 pp.

Brown, G. S., H. R. Stanley, and N. A. Rey, 1981: The wind speed measurement capability of space borne radar altimeters. *IEEE J. Oceanic Eng., OE-6*(2), 59–63.

Chelton, D. B., E. J. Walsh, and J. F. Mac Arthur, 1989: Pulse compression and sea level tracking in satellite altimetry. *J. Atmos. Oceanic Technol.*, **6**, 407–438.

Cheney, R. E., B. C. Douglas, R. W. Agreen, L. Miller, D. L. Porter, and N. S. Doyle, 1987: Geosat altimeter geophysical data record user handbook. NOAA Tech. Memo. NOS NGS-46, 29 pp.

——, B. C. Douglas, and L. Miller, 1989: Evaluation of Geosat altimeter data with application to tropical Pacific sea level variability. *J. Geophys. Res.*, **94**, 4737–4747.

Dobson, E. B., F. M. Monaldo, J. Goldhirsh, and J. Wikerson, 1987: Validation of Geosat altimeter-derived wind speeds and significant wave heights using buoy data. *J. Geophys. Res.*, **92**, 10 719–10 731.

Douglas, B. C., and R. W. Agreen, 1983: The sea state correction for GEOS 3 and Seasat altimeter data. *J. Geophys. Res.*, **88**, 1655–1661.

——, and R. E. Cheney, 1988: Geosat electromagnetic bias analysis. US WOCE Tech. Rep. 2, D. Chelton, Ed., 70 pp.

Fu, L., and R. E. Glazman, 1991: The effect of the degree of wave development on the sea-state bias in radar altimetry measurements. *J. Geophys. Res.*, **96**, 829–834.

Glazman, R. E., and S. H. Pilorz, 1990: Effects of sea maturity on satellite altimeter measurements. *J. Geophys. Res.*, **95**, 2857–2870.

——, G. G. Pihos, and J. Ip, 1988: Scatterometer wind speed bias induced by the large-scale component of the wave field. *J. Geophys. Res.*, **93**, 1317–1328.

Guymer, T., and M. A. Srokosz, 1988: The determination of sea-state bias and non-linear wave parameters from satellite altimeter data. *Proc. Earsel Symp. ESA SP-258*, European Space Agency, Alpbach, 115–120.

Hayne, G. S., and D. W. Hancock, 1982: Sea state related altitude errors in the Seasat radar altimeter. *J. Geophys. Res.*, **87**, 3227–3231.

Jourdan, D., Ch. Boissier, A. Braun, and J. F. Minster, 1990: Effect of wet tropospheric correction on the estimation of mesoscale dynamic topography by altimetry. *J. Geophys. Res.*, **95**, 17 993–18 004.

Katsaros, K. B., and R. M. Lewis, 1986: Mesoscale and synoptic scale features of North Pacific weather systems observed with the Scanning Multichannel Microwave Radiometer of *Nimbus-7*. *J. Geophys. Res.*, **91**, 2321–2230.

Lagerloef, G. S. E., 1987: Comment on "The joint distribution of surface elevations and slope for a non linear random sea, with application for radar altimetry" by M. A. Srokosz. *J. Geophys. Res.*, **92,** 2985–2987, 1987.

Le Traon, P. Y., M. C. Rouquet, and Ch. Boissier, 1990: Spatial scales typical of mesoscale variability in the North Atlantic, as deduced from Geosat data, *J. Geophys. Res.*, **95,** 20 267–20 286.

Marty, J. C., and A. Cazenave, 1988: Thermal evolution of the lithosphere beneath fracture zones inferred from geoid anomalies. *Geophys. Res. Lett.*, **15,** 593–596.

Melville, W. K., R. H. Stewart, W. C. Keller, J. A. Kong, D. V. Arnold, A. T. Jessup, M. R. Loewen, and A. M. Slinn, 1991: Measurements of electromagnetic bias in radar altimetry. *J. Geophys. Res.*, **96,** 4915–4924.

Minster, J. F., L. P. Ricard, and C. J. Allegre, 1979: ^{87}Rb-^{87}Sr chronology of enstatite meteorites. *Earth Planet. Sci. Lett.*, **44,** 420–440.

Mognard, N., 1984: Swell in the Pacific Ocean observed by SEASAT radar altimeter. *Marine Geod.*, **8,** 183–210.

Monaldo, F., 1990: Path length variations caused by atmospheric water vapor and their effects on the measurement of mesoscale ocean circulation features by a radar altimeter. *J. Geophys. Res.*, **95,** 2923–2932.

Nerem, R. S., B. D. Tapley, and C. K. Shum, 1990: Determination of the ocean circulation using Geosat altimetry. *J. Geophys. Res.*, **95,** 3163–3179.

Ray, R. D., and C. J. Koblinsky, 1991: On the sea-state bias of the GEOSAT altimeter, *J. Atmos. Oceanic Technol.*, **8,** 397–408.

Rodriguez, E., 1988: Altimetry for non-Gaussian oceans: Height biases and estimation of parameters. *J. Geophys. Res.*, **93,** 14 107–14 120.

Srokosz, M. A., 1986: On the joint distribution of surface elevation and slopes for a non linear random sea, with application to radar altimetry. *J. Geophys. Res.*, **91,** 995–1006.

Stewart, R., 1988: A review of sea-state bias in altimetry, US WOCE Tech. Rep. 2, D. Chelton, Ed., 70 pp.

Walsh, E. J., F. C. Jackson, E. A. Uliana, and R. N. Swift, 1989: Observations of electromagnetic biases in radar altimeter sea surface measurements. *J. Geophys. Res.*, **94,** 14 107–14 120.

Wendt, I., and C. Carl, 1991: The statistical distribution of the mean squared weighted deviation. *Chemical Geol.*, **86,** 275–285.

Yaplee, B. S., A. Shapiro, D. L. Hammond, B. B. Au, and E. A. Uliana, 1971: Nanosecond radar observation of the ocean surface from a stable platform, *IEEE Trans. Geosci. Electron.*, GE-**9,** 170–174.

Zlotnicki, V., L. L. Fu, and W. Patzert, 1989: Seasonal variability in global sea level observed with Geosat altimetry. *J. Geophys. Res.*, **94,** 959–969.